Northumbria Research Link

Citation: Zharkova, Valentina and Dobranskis, Rytis (2016) Updated analytical solutions of continuity equation for electron beams precipitation - II. Mixed energy losses. Monthly Notices of the Royal Astronomical Society, 458 (4). pp. 3720-3730. ISSN 0035-8711

Published by: Oxford University Press

URL: https://doi.org/10.1093/mnras/stw500 <https://doi.org/10.1093/mnras/stw500>

This version was downloaded from Northumbria Research Link: http://nrl.northumbria.ac.uk/id/eprint/26871/

Northumbria University has developed Northumbria Research Link (NRL) to enable users to access the University's research output. Copyright © and moral rights for items on NRL are retained by the individual author(s) and/or other copyright owners. Single copies of full items can be reproduced, displayed or performed, and given to third parties in any format or medium for personal research or study, educational, or not-for-profit purposes without prior permission or charge, provided the authors, title and full bibliographic details are given, as well as a hyperlink and/or URL to the original metadata page. The content must not be changed in any way. Full items must not be sold commercially in any format or medium without formal permission of the copyright holder. The full policy is available online: http://nrl.northumbria.ac.uk/policies.html

This document may differ from the final, published version of the research and has been made available online in accordance with publisher policies. To read and/or cite from the published version of the research, please visit the publisher's website (a subscription may be required.)

Northumbria University NEWCASTLE

University Library

Mon. Not. R. Astron. Soc. **000**, 000–000 (0000) Printed 26 May 2016 (MN LATEX style file v2.2)

Updated analytical solutions of continuity equation for electron beams precipitation - II. Mixed energy losses

V. V. Zharkova⋆ and R. R. Dobranskis
Department of Mathematics and Information Sciences, University of Northumbria, Newcastle upon Tyne, NE1 2XP, UK

Received 2015 October 4

ABSTRACT
In this paper we consider simultaneous analytical solutions of continuity equations for electron beam precipitation a) in collisional losses and b) in Ohmic losses, or mixed energy losses (MEL), by applying the iterative method to calculate the resulting differential densities at given precipitation deph. The differential densities of precipitating electrons derived from the analytical solutions for mixed energy losses reveal increased flattening at energies below 10-30 keV compared to a pure collisional case. This flattening becomes stronger with an increasing precipitation depth turning into a positive slope at greater precipitation depths in the chromosphere resulting in a differential density distribution with maximum that shifts towards higher energies with increase of a column depth. While the differential densities combining precipitating and returning electrons are higher at lower energies than those for a pure collisional case. The resulting hard X-ray (HXR) emission produced by the beams with different initial energy fluxes and spectral indices is calculated using the MEL approach for different ratios between the differential densities of precipitating and returning electrons. The number of returning electrons can be even further enhanced by a magnetic mirroring, not considered in the present model, while dominating at lower atmospheric depths where the magnetic convergence and magnitude are the highest. The proposed MEL approach provides an opportunity to account simultaneously for both collisional and ohmic losses in flaring events, which can be used for a quick spectral fitting of HXR spectra and evaluation of a fraction of returning electrons versus precipitating ones. The semi-analytical MEL approach is used for spectral fitting to RHESSI observations of nine C, M and X class flares revealing a close fit to the observations and good resemblance to numerical FP solutions.

Key words: plasmas – Sun: atmosphere – Sun: flares – Sun: particle emission – Sun: X-rays, gamma rays.

1 INTRODUCTION

It is well established that during solar flares, non-thermal electron beams are accelerated somewhere at coronal atmospheric levels, and precipitate into the lower atmosphere depositing their energy into the ambient plasma. The non-thermal electrons lose their energy in collisions and ohmic energy loses while producing bremsstrahlung hard X-ray emission. Also a massive amount of non-thermal energy released by accelerated particles is converted into the ambient plasma heating producing strong soft X-ray, ultra-violet and optical emission.

Numerous observations of solar flares in a wide range of electromagnetic spectra have provided a valuable insight on the internal processes within the solar flares, leading to the development of different particle transport and energy loss models. The most energetic emission produced by solar flares, hard X-ray (HXR) and γ-ray spectra, are investigated with Reuven Ramaty High-Energy Solar Spectroscopic Imager (*RHESSI*) (Lin et al. 2002) with the finest angular and spectral resolutions. Imaging spectroscopy analysis of this data is used as a powerful tool to explore the underlying physics of particle acceleration and transport in solar flares.

Different methods are used to interpret the observed spectra of energetic particles; the most accepted are the analytical solutions for energy spectra of precipitating electrons derived from for pure collisional energy losses the inversion of hard X-ray bremsstrahlung spectra of precipitating electron beams (Brown 1971, 1972) or from the direct solutions of continuity equations (Syrovatskii & Shmeleva 1972). Electron beams precipitating into flaring atmosphere are also found to induce an electrostatic electric field leading to sub-

⋆ E-mail:valentina.zharkova@northumbria.ac.uk

© 0000 RAS

stantial Ohmic losses for precipitating electrons (Knight & Sturrock 1977; Emslie 1980; Diakonov & Somov 1988). This electric field at the same time was assumed to produce a return current mostly from the ambient electrons.

Although Zharkova & Gordovskyy (2006) have shown analytically that the self-induced electric field also forms returning electrons from the precipitating ones. Energy losses in electric field are found to substantially decrease a precipitation depth of precipitating electrons (Zharkova & Gordovskyy 2006), then a number of low energy (<100 keV) electrons is also substantially decreased, when Ohmic losses are considered (Diakonov & Somov 1988; Zharkova et al. 1995; Zharkova & Gordovskyy 2006; Sui et al. 2007). This can lead to the electron beams with a greater initial energy flux to induce a stronger electric field and, thus, to have higher Ohmic losses (Zharkova & Gordovskyy 2006; Sui et al. 2007).

In order to consider mixed energy losses for electron precipitation the numerical methods are required. This includes the solution of a Fokker-Planck equation for collisional losses in converging magnetic field by Leach & Petrosian (1981) or for combined collisional and Ohmic losses in converging magnetic field(McClements 1992; Syniavskii & Zharkova 1994; Zharkova et al. 1995).

However, full understanding of the role of a self-induced electric field in electron beam dynamics came only from the simulation in the Fokker-Planck (FP) approach of the time-dependent injection of power law electrons (Siversky & Zharkova 2009). The authors for the first time derived that the main part of returning electrons is formed from precipitating electrons scattered to pitch angles with negative cosines (or returning beam electrons). This approach is essentially different from the earlier one (Knight & Sturrock 1977) considering a return current formed by the ambient electrons.

Using the Fokker-Planck approach to calculate distribution functions of electron beams precipitating into a flaring atmosphere, Siversky & Zharkova (2009) showed that precipitating and returning beam electrons form an electric circuit from the corona to the photosphere where the beam electrons are recycled, or, travel many times up and down while injection continues. The characteristic time-scale for the creation of this electric circuit is 0.07-0.1 s, while the travel time of relativistic beam electrons from the corona to the photosphere is about 0.01 -0.1 s. This means that after the circuit is established the beam electrons can make up to 10-100 journeys downward and upward resolving the particle number problem because only (1-10)% of accelerated electrons can account for the observed HXR photon numbers.

Further progress with high-resolution observations, made by the RHESSI payload, have provided the data leading to better understanding of photon and electron spectra emitted during solar flares and to deriving the exact locations and shapes of HXR sources on the solar disc where they occur (Brown et al. 2006; Krucker et al. 2008). Many powerful flares are found to produce the elbow-type HXR photon spectra with double power-law energy distributions (Kontar et al. 2002; Conway et al. 2003; Holman et al. 2003), which cannot be completely explained by purely collisional energy losses.

Initially, the flattening of HXR photon spectra was explained by purely collisional model with an increased lower cut-off energy by shifting it to the turning point where HXR emission flattens (**?**)or by the partial HXR albedo effect at its reflection from the photosphere (Massone et al. 2004). However, these previous studies have empasized the importance of considering multiple energy loss mechanisms, particularly, inclusion of the self-induced electric field of precipitating electrons (Sui et al. 2007).

Zharkova & Gordovskyy (2006); Sui et al. (2007); Siversky & Zharkova (2009) shown that ohmic losses can be the most likely reason causing this flattening because electron beams with the greater initial energy flux induce stronger electric fields and, thus, have higher ohmic losses for lower energy electrons. This leads to a greater flattening of their photon spectra at lower energies. Since, a number of low energy (<100 keV) precipitating electrons is substantially decreased if both Coulomb collisions and ohmic losses are considered. This causes flattening of energy spectra of electrons at lower energy, that can be a rather logical interpretation of an elbow-type HXR spectrum. This, in turn, allows us to estimate photon spectra, directivity and polarisation with close resemblance to the HXR and microwave (MW) observations (Zharkova et al. 2010, 2011).

Of course, in a converging magnetic field of loop legs more electrons can be returned back to the corona by magnetic mirroring effect (Leach & Petrosian 1981, 1983; Zharkova et al. 1995; Siversky & Zharkova 2009). Indeed, Siversky & Zharkova (2009) have indicated (see their Fig. 7 and 8) that the beam electrons are returned back to the corona by a converging magnetic field with the number of returned electrons increasing with a precipitation depth when the convergence factor and absolute magnitude of magnetic field are progressively increased following the convergence formulae (36 -37) in Siversky & Zharkova (2009)). In the other words, a number of the mirrored electrons in the upper corona is much smaller than those from the upper or middle chromosphere. Moreover, from all the 4 forms of the definition of magnetic convergence available in the current literature, the only one derived from the observations seems to fit best the observed magnetic field magnitudes measured in the chromosphere and photosphere (Siversky & Zharkova 2009).

Using this approach, it was shown from a comparison of the theoretical and observed HXR and MW emission (Zharkova et al. 2010, 2011) that the magnetic mirroring affects noticeably only those electrons with higher energy above a hundred keV which reach deeper atmospheric levels where the magniture and convergence factor of magnetic field are higher. At the same time, the mirroring of lower energy electrons occurs at upper atmospheric depths where the magnetic field and convergence factor magnitudes are low that results in a lower fraction of the mirrorred electrons with lower energies at these depths. While the return current is produced by the self-induced electric field of beam electrons immediatelly after the beam injection in the top of the corona. This return current is mostly formed by the electrons with the energies below 80 keV (Zharkova et al. 1995; Siversky & Zharkova 2009; Zharkova et al. 2011). It becomes evident that a return current and magnetic mirroring are the complementary effects defining electron distributions and their high energy emission at different precip-

itating depths (Siversky & Zharkova 2009; Zharkova et al. 2011).

Given the fact that the beam electrons are assumed to have power law energy distributions, ($E^{-\gamma}$), the bulk of beam electrons is defined by those electrons with lower energies below 100 keV. These lower energy electrons, in turn, primarily define the electrc circuit and return current formed by precipitating and returning electrons, while only a small fraction ($\approx E^{-\gamma}$) of higher energy electrons can be affected by magnetic mirroring. Hence, the magnetic mirroring effects can increase a number of higher energy electrons in the population of returning electrons and, thus, can reduce a spectral index of their resulting HXR emission at higher energies (Zharkova et al. 2010, 2011), contrary to the ohmic losses reducing the HXR spectral indices at lower energies (Siversky & Zharkova 2009).

With all the significant progress in the interpretation of HXR and MW emission, the numerical Fokker-Planck approach is rather complex and requires extensive calculations, while observers of photon spectra with RHESSI or FERMI payload would prefer to have a quick analytical tool for their interpretation. Hence, an alternative semi-analytical approach considering Coulomb collisions and ohmic energy losses with a reduced computational time can be very useful. This approach can be also extended in the future interpretation by adding the analytical solutions for magnetic mirroring of beam electrons, similar to the analytical approach considered by Zharkova & Gordovskyy (2005).

In the current paper we propose an iterative semi-analytical method for the initial investigation of electron beam parameters by combining the analytical solutions for mixed energy losses (MEL). e.g. pure collisional and pure Ohmic losses reported in Part 1 (Dobranskis & Zharkova 2015). The outcome of this method for electron distribution functions is benchmarked by a FP approach and compared with the HXR spectra observed in a few flares.

The iterative method for calculation of differential densities of beam electrons for mixed energy losses (MEL) is described in section 2, their resulting hard-X-ray intensities are presented in section 3, a comparison of simulated spectra with HXR photon spectra observed for a number of flares are discussed in section 3.2 and conclusions are drawn in section 4.

2 DIFFERENTIAL SPECTRA OF ENERGETIC ELECTRONS FOR MIXED ENERGY LOSSES (MELS)

Hard X-rays is bremsstrahlung emission produced by collisions of precipitating beam electrons with the ambient plasma electrons or ions. The loss of energy of precipitating electrons in ohmic losses, on the one hand, reduces the energy of precipitating electrons, and, on the other hand, it changes a direction of motion of low energy electrons so that some part of them is reversed to a return current (Zharkova & Gordovskyy 2006; Dobranskis & Zharkova 2015). These can have a significant effect on HXR intensity distribution, producing spectral flattening at lower energies (Zharkova & Gordovskyy 2006; Siversky & Zharkova 2009).

However, for simplicity, the classic collisional approach (Brown 1971, 1972; Syrovatskii & Shmeleva 1972) is implemented in the RHESSI software to fit the observed photon energy spectra, which gives the first views of electron precipitation in flares. It would be a great advantage for observers to have an analytical or semi-analytical method considering not only collisional but also ohmic losses that can be used for the initial estimation of the contribution of these mechanisms into electron beam distributions over a precipitation depth.

This can give researchers an initial idea on the role of ohmic energy loses in the particular flare, while the outcome of the analytical estimations can be later compared with the results found from the numerical Fokker-Planck solutions. This can be achieved using the analytical solutions found from continuity equations for pure collisional and pure ohmic losses reported in paper 1 (Dobranskis & Zharkova 2015) by applying them iteratively as described below.

2.1 The iterative method of solution

The continuity equation for mixed energy losses cannot be analytically integrable. However, the approximated solution of CE for mixed energy loses can be found with an using iterative method proposed here, by deploying the analytical solutions found in the part I of this research (Dobranskis & Zharkova 2015) for each energy loss mechanism. The differential densities (DDs) for lixed energy losses are derived from the updated solutions of continuity equations for collisional and ohmic losses as follows.

2.1.1 Differential densities for pure collisions

Differential densities obtained from the updated CE solutions for Coulomb collisions are described by the expression (25) in Dobranskis & Zharkova (2015):

$$N(E,\xi)_{Coll} = K_N\sqrt{E}\left(E^2+2a\xi\right)^{-\frac{\gamma+1}{2}} \times \Theta\left(\sqrt{E^2+2a\xi}-E_{low}\right) \times \Theta\left(E_{upp}-\sqrt{E^2+2a\xi}\right), \quad (1)$$

where K_N is a normalisation constant, a is the collisional coefficient, Θ represents the Heavyside step function, and ξ is the column depth:

$$\xi(x) = \int_0^x n(t)\,dt, \quad (2)$$

which defines a total number of particles in the line of sight, within the area of one square centimetre.

2.1.2 Differential densities of precipitating electrons for pure ohmic losses

Differential desnities of precipitating electrons obtained from the updated CE for ohmic losses can be described by the expression (40) in Dobranskis & Zharkova (2015):

$$N(E,s)_{OhmP} = K_N E^{-\frac{1}{2}}(E+e\mathcal{E}s_i)^{-\gamma} \times \Theta\left[(E+e\mathcal{E}s_i)-E_{low}\right]\Theta\left[E_{upp}-(E+e\mathcal{E}s_i)\right], \quad \mu=+1, \quad (3)$$

where $\mathcal{E}$ is the self-induced electric field and s is a linear precipitation depth.

2.1.3 Differential densities of returning electrons for pure ohmic losses

Differential densities of 'returning electrons' derived from the updated CE solutions for purely ohmic losses is described by the expression (41) in Dobranskis & Zharkova (2015):

$$N(E,s)_{OhmR} = K_N E^{-\frac{1}{2}} (E + e\mathcal{E}s_i)^{-\gamma} \times \Theta\left[E_{upp} - E - e\mathcal{E}s_i\right], \ \mu = -1, \quad (4)$$

2.1.4 Iterative steps

(i) As the first step, let us use the updated CE equation (1) for purely collisional losses to estimate the differential density ($N(E,\xi)_{Coll}$) at the initial column depth (ξ).

(ii) This differential density ($N(E,\xi)_{Coll}$) is used to calculate electron beam energy flux $F(E,\xi)$ which is required to to estimate the induced electric field at a column depth (ξ) as follows:

$$\mathcal{E}(\xi) = \frac{e}{\sigma} \int_{E_{low}}^{E_{upp}} F(E,\xi)\, dE, \quad (5)$$

where σ defines the ambient plasma conductivity, and $F(E,\xi)$ refers to an electron beam energy flux, found from the differential density at a given column depth.

Thus, we estimate the electric field from the updated CE solution (equation 3) for collisional losses, which is then used as a parameter in the DD solution for ohmic losses.

(iii) At each step the electron energies used in the updated CE solutions for ohmic losses are adjusted to reflect at the same step the energy losses in collisions.

(iv) Then in the next step electron energies for collisional solutions are adjusted to fit the DDs found for ohmic losses at the previous step and so on.

(v) This process is repeated for every column depth.

Using this approach one obtains the simultaneous solutions for precipitating and returning electrons considering analytical solutions for pure collisions and ohmic losses for precipitating electrons (case 1) and for returning electrons (case 2). The results of DD calculations are discussed in the subsections below.

2.2 Results: differential densities for precipitating electrons

Differential densities for precipitating beam electrons losing energy in Coulomb collisions and ohmic losses are plotted in Fig. 1. The injected electron beams have the following parameters: the initial energy flux of $F_0 = 10^{10}\ erg \cdot s^{-1}$ (supplementary Fig. 1, top plots) and $F_0 = 10^{12}$ erg cm^{-2} (supplementary Fig. 1, bottom row plots), and the spectral indices $\gamma = 3$ (and supplementary Fig. 1, left column) and 7 (Fig. 1 and supplementary Fig. 1, right column).

The electric field is considered to be variable, having the initial value $\mathcal{E}_0 = 5 \times 10^{-5}$ V/cm for less intense electron beams (top row), and increasing to $\mathcal{E}_0 = 3 \times 10^{-3}$ V/cm for more powerful beams (bottom row). The energy spectra are constrained by the lower $E_{low} = 12$ keV and the upper $E_{upp} = 2$ MeV cut-off energies. The results are plotted for the column depth range from $\xi = 2.8 \times 10^{18}$ (upper curve) to 5.1×10^{20} cm^{-2} (bottom curve).

As expected, the differential densities (DDs), estimated for electron beams precipitating in MEL, considering the additional energy losses in the electric field, are significantly lower than the ones obtained for purely collisional case and strongly depend on the beam's initial flux and spectral index. The differential densities of a moderately intense electron beams with a lower initial flux F_0 (supplementary Fig. 1a,b) show stronger (by the order of the magnitude) decrease of electrons with lower energies at the smaller precipitating depth, while at deeper atmospheric depths the differences are nearly negligeable for a harder beam (γ=3) and still noticeable for the softer one (γ=7). And for a stronger electron beams with the higher initial flux F_0 (supplementary Fig. 1c,d), which have much greater energy losses caused by the self-induced electric field, there is a significant (by a few orders of the magnitude) decrease of differential densities of beam electrons at lower energies calculated for MEL losses compared to the pure collisional ones.

In general, the differential densities calculated for MELs have distributions with the positive slopes towards lower energies than for pure collisional losses with the slopes increasing with the precipitation depth (compare the curves at energies below 3 keV (blue) or below 30 keV (red)) forming wide maxima at greater depths in the chromosphere. The electron beams loosing their energy in MELs have steeper positive slopes and more pronounced maxima, than the ones loosing their energy in purely Coulomb collision that resembles the findings of numerical solutions with FP (Siversky & Zharkova 2009). The maximum shifts towards higher energies with the increase of a column depth, e.g. approximately the two orders of a magnitude increase in column depth (from 2.8×10^{18} to 5.1×10^{20} cm^{-2}) would shift the maximum from 4 keV to 21 keV (Fig.1).

The differential density distributions presented for lower $\gamma = 3$ (supplementary Fig.1a,c) and higher $\gamma = 7$ (supplementary Fig.1b,d) spectral indices show that for harder beams there are smaller differences between the differential densitiess calculated for MEL and pure collisional case than for the beams with higher spectral index. This happens because the electric field responsible for ohmic losses is induced by the precipitating electrons themselves. Thus, it is proportional to the initial energy flux of a beam, leading to higher ohmic losses for more intense beams and has much more complex dependence on their spectral index as shown in formulae (1) and (3). This results in a lower magnitudes and increased positive slopes of differential density of beam electrons at given depths for the MEL losses for harder and more intense beams and leads to the maxima moving to higher energies for softer beams that can be essential for the generation of plasma turbulence.

2.3 Results: differential densities for returning electrons

It was demonstrated by Fokker-Planck approach (Siversky & Zharkova 2009), that a large fraction of precipitating elec-

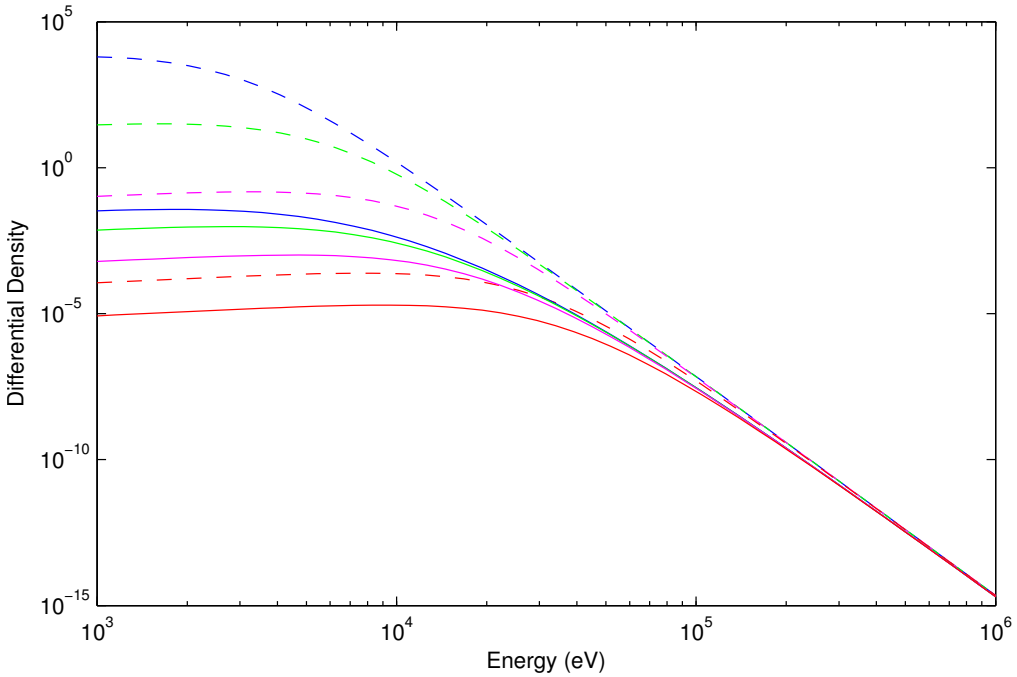

(a) $F_0 = 10^{12} erg\, cm^{-2} s^{-1}, \gamma = 7$

Figure 1. Differential densities of precipitating electron beams calculated for MEL (Coulomb collisions + ohmic losses) (the solid lines) for beam electrons with energies in a range of 16-384 keV, at the column depths of ξ of 2.8 $\times$ 10^{18} cm $^{-2}$ (blue), 1.3 $\times$ 10^{19} cm^{-2} (green), 7.6 $\times$ 10^{19} cm^{-2} (magenta) and 5.1 $\times$ 10^{20} cm^{-2} (red). For comparison, differential densities of electron beams with the same parameters losing their energy in Coulomb collisions are plotted by dashed lines.

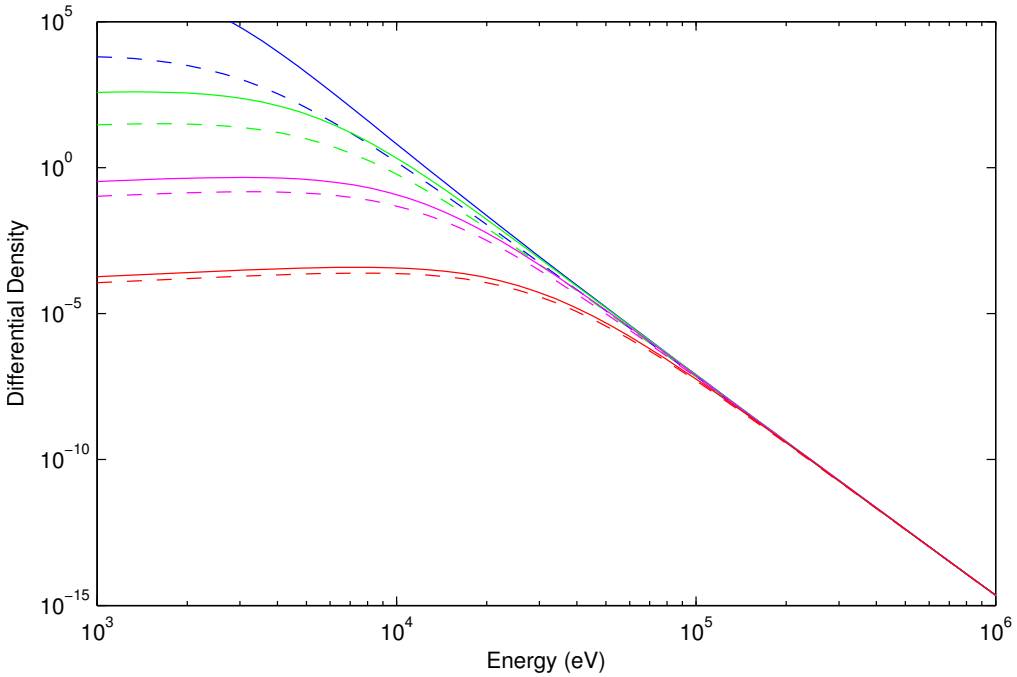

(a) $F_0 = 10^{12} erg\, cm^{-2} s^{-1}, \gamma = 7$

Figure 2. Differential densities of electron beams derived for precipitating electrons losing their energy in Coulomb collisions plus returning electrons (solid lines)in comparison with differential densities calculated for pure collisions (dashed lines). Results are presented at the same column depths as in Fig. 1 for beam electrons with the energy range of 12 keV- 2 MeV. The colour schemes of the curves correspond to the depths described in Fig. 1.

trons can be turned by their own electric field back to the top in the corona where they are injected from. As we discovered in section 2.2, the distributions of returning electrons are substantially different from those of the precipitating electrons losing their energy in electric field.

In order to estimate the effect of returning electrons on hard X-ray emission emitted upwards to the corona, let us investigate the differential densities of electrons for a combination of electron beams losing their energy in Coulomb collisions at given depth (equation 1) and returning electrons (equation 4) gaining their energy in a self-induced electric field. The variations of the resulting differential densities are presented in Fig. 2 for the initial energy flux $F_0 = 10^{12}$ $erg \cdot cm^{-2}s^{-1}$ and γ=7 and in the supplementary Fig. 2 for hard $\gamma = 3$ (supplementary Fig.2a,c) and soft $\gamma = 7$ (supplementary Fig.2b,d) electron beams with the initial energy fluxes of 10^{10} $erg/cm^2/s$ (supplementary Fig.2a,b) and 10^{12} $erg/cm^2/s$ (supplementary Fig.2c,d).

The resulting differential densities at every precipitation depth of combined precipitating and returning electrons are higher than those for purely collisional case because the returning electrons being accelerated by the electric field increase the number of electrons at given depth because they gain energy in this electric field and increase the resulting differential density for MEL. The impact of an electric field magnitude on differential density distributions is compared in the supplementary Fig. 2 (top row), where the electron beams induce the self-induced electric field of moderate magnitude of ($\mathcal{E}_0 = 7 \times 10^{-6}$ V/cm), in the suplementary Fig. 2 (bottom row) calculated for a stronger electric field magnitude ($\mathcal{E}_0 = 3 \times 10^{-3}$ V/cm).

Again, similar to the precipitating electrons shown in Fig. 1, the increase of differential density at given precipitating depth in the "returning" electrons is more significant for more powerful electron beams, due to a very strong self-induced electric field produced by such the beams. An increase of the electric field magnitude results in some flattening of the positive slope formed by precipitating electrons at lower energies, especially at the deeper atmospheric depths, from where the returning electrons gain the largest amount of energy. This increase, in fact is comparable with but slighly lower then the decrease of DDs for precipitating electrons described in section 2.2.

While the dependence of DDs for precipitating plus returning electrons on spectral indices are much more complicated following the formulae (1) and (4). At higher atmospheric levels, or lower precipitation depths, the increase of returning electronsbecomes extremely significant approaching one order of the magnitude for harder beams (γ=3), 3 orders of magnitude for softer moderate beams (γ=7) and 4 orders of the magnitude for a softer stronger beam (Fig. 2). Although, with the increase of a precipitation depth beyond the stopping depth of electrons with lower cutoff energy (12 keV), the densities of returning electrons become negligeable leading to the same differential densities as for the precipitating electrons only shown in Fig. 1.

2.4 Fractions of precipitating and returning electrons

In order to estimate accurately the ratios between the numbers of precipitating ($\mu = +1$) and returning ($\mu = -1$) electrons from a total number injected, let us use the solutions obtained from numerical Fokker-Planck approach (FPA) (Siversky & Zharkova 2009). The ratio can be expressed as a percentage of precipitating electrons present at a certain column depth from the total number of electrons (100%) including precipitating and returning ones. This ratio is found to be dependent on electron beam parameters as outlined in Tables 1, 2 and 3 showing its variations for

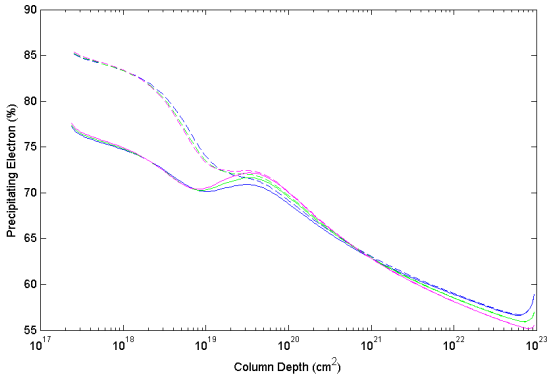

(a) $F_0 = 10^8 erg\, cm^{-2}s^{-1}$

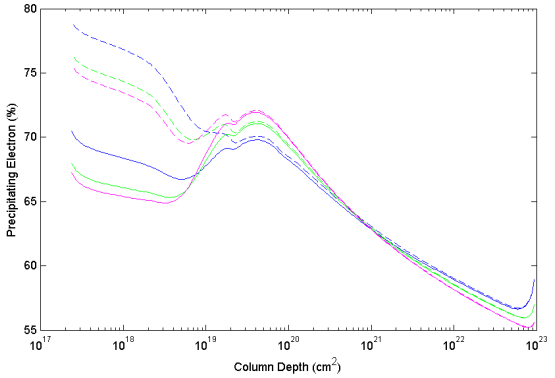

(b) $F_0 = 10^9 erg\, cm^{-2}s^{-1}$

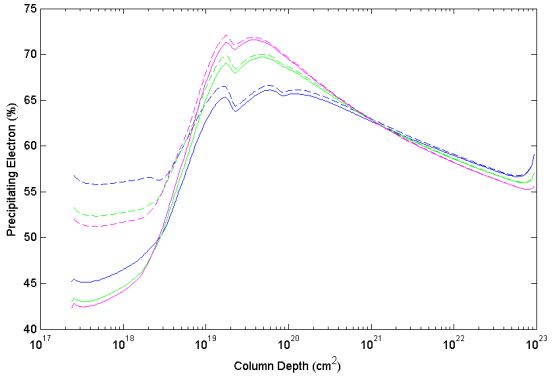

(c) $F_0 = 10^{10} erg\, cm^{-2}s^{-1}$

Figure 3. Variations with a column depth of precipitating electron ratio derived from Fokker-Planck approach for electron beams with spectral index $\gamma = 3$ (blue), $\gamma = 5$ (green) and $\gamma = 7$ (magenta). The solid lines are used for the pitch angle dispersion at injection of $\Delta\mu = 0.2$ and dashed lines for $\Delta\mu = 0.02$.

Table 1. Fraction of precipitating electrons at $\xi = 2.4 \times 10^{17}$ cm^{-2}

γ	3		5		7	
$\Delta\mu$	0.2	0.02	0.2	0.02	0.2	0.02
$F = 10^8$	77.2%	85.4%	77.4%	85.5%	77.6%	85.6%
$F = 10^9$	70.5%	79.0%	68.0%	76.5%	67.2%	75.6%
$F = 10^{10}$	45.2%	56.7%	43.0%	53.00%	42.3%	51.8%

Table 2. Fraction of precipitating electrons at $\xi = 2.5 \times 10^{18}$ cm^{-2}

γ	3		5		7	
$\Delta\mu$	0.2	0.02	0.2	0.02	0.2	0.02
$F = 10^8$	73.1%	81.4%	73.0%	81.2%	73.2%	81.1%
$F = 10^9$	67.5%	75.3%	65.6%	72.9%	65.0%	72.0%
$F = 10^{10}$	49.4%	56.4%	48.9%	54.0%	49.1%	53.6%

different initial energy fluxes F, spectral indices γ and the pitch angle dispersion $\Delta\mu$.

From Table 1 one can derive that on the top of the atmosphere ($\xi = 2.4 \times 10^{17}$ cm^{-2}), weak electron beams ($F = 10^8$ erg cm^{-2} s^{-1}) have highest percentage of precipitating electrons (77.23% for $\gamma = 3$, $\Delta\mu = 0.2$), which becomes only slightly higher for softer electron beams (77.58% $\gamma = 7$). A smaller pitch angle dispersion ($\Delta\mu$) at injection of beam electrons (defining beams directed closer to the direction μ=1) leads to a further increase by approximately 8% (from 77% to 85%), allowing for 15-23% of the number returning electrons, reducing thus the number of precipitating electrons.

Table 3. Fraction of precipitating electrons at $\xi = 2.4 \times 10^{19}$ cm^{-2}

γ	3		5		7	
$\Delta\mu$	0.2	0.02	0.2	0.02	0.2	0.02
$F = 10^8$	70.8%	71.8%	71.5%	72.1%	71.9%	72.4%
$F = 10^9$	69.2%	69.6%	70.3%	70.5%	71.2%	71.3%
$F = 10^{10}$	63.9%	64.5%	68.2%	68.6%	70.7%	71.1%

In case of powerful electron beam with the initial energy flux ($F = 10^{12}$ erg cm^{-2} s^{-1}) and small $\gamma = 3$, $\Delta\mu = 0.2$), a stronger self-induced electric field is generated. This results in a larger number of returning electrons moving towards the corona, or in a much lower percentage (45.21% of precipitating electrons. The increase of spectral index leads to increase of electric field and thus, to a decrease of percentage of precipitating electrons (by 3%). While a lower pitch angle dispersion ($\Delta\mu$) increases this percentage by approximately 9-11% (from 45% to 56% for $\gamma = 3$, or from 42% to 51% for $\gamma = 7$), allowing for 43-57% of the returning electrons, depending on spectral index and angle of dispersion.

Further investigation of Tables 2, 3 and Fig.3 reveals that electron beams with a very weak initial energy flux, e.g. $F = 10^8$ (Fig.3a), 10^9 (Fig.3b) erg cm^{-2} s^{-1}, and smaller pitch angle dispersion $\Delta\mu = 0.02$ have the highest percentage of precipitating electrons at the upper atmospheric level while this number decreases exponentially with the increase of a column depth.

On the other hand, the maximum in the percentage of precipitating electrons shifts deeper into the atmosphere (from $\xi = 10^{17}$ cm to 5.0^{19} cm) with the increase of the initial energy flux F, which means that a significant number of electrons reaches the chromospheric levels. The shifted maximum first becomes clearly visible in Fig. 3b ($F = 10^9$ erg cm^{-2} s^{-1}, $\Delta\mu = 0.2$). While, in the case of $F = 10^{10}$ erg cm^{-2} s^{-1} (Fig.3c) the maximum is well pronounced for both magnitudes of a pitch-angle dispersion $\Delta\mu = 0.2$ and 0.02.

Similar to FP solutions (Siversky & Zharkova 2009), in the iterative use of the analytical solutions for collisional and Ohmic losses, a magnitude of an initial energy flux, F, of beam electrons has the most significant impact on the density ratios of precipitating-to-returning electrons at all column depths. While the variations of a pitch angle dispersion has a significant effect only at higher atmospheric levels up to $\xi = 2.0 \times 10^{19}$ cm^{-2}, and they are 8% higher for narrower beams with $\Delta\mu = 0.02$). At deeper atmosphere electrons become strongly thermalised approaching nearly isotropic distribution at the lower chromosphere levels.

Additionally, continuity equations for purely collisional (formula 1) and ohmic (formula 3) energy losses, are integrated by energy in the following way:

$$N(\xi) = K_N \int_{E_{low}}^{E_{upp}} \sqrt{E}\left(E^2 + 2a\xi\right)^{-\frac{\gamma+1}{2}} dE = \\ = \frac{K_N \times 2^{\frac{1-\gamma}{2}}}{3} E^{\frac{3}{2}} \left(\frac{E^2}{a\xi} + 2\right)^{\frac{\gamma+1}{2}} \left(E^2 + 2a\xi\right)^{-\frac{\gamma+1}{2}} \\ \times \left(\sum_{n=0}^{\infty} \frac{(0.75)_n \left(\frac{\gamma+1}{2}\right)_n}{(1.75)_n} \frac{\left(-\frac{E^2}{2a\xi}\right)^n}{n!}\right) |_{E_{low}}^{E_{upp}} \quad (6)$$

$$N(s) = K_N \int_{E_{low}}^{E_{upp}} E^{-0.5} \left(E + e\mathcal{E}s_i\right)^{-\gamma} dE = \\ = 2K_N \sqrt{E} \left(\frac{E}{e\mathcal{E}s_i} + 1\right)^{\gamma} \left(E + e\mathcal{E}s_i\right)^{-\gamma} \\ \times \left(\sum_{n=0}^{\infty} \frac{(0.5)_n (\gamma)_n}{(1.5)_n} \frac{\left(-\frac{E}{e\mathcal{E}s_i}\right)^n}{n!}\right) |_{E_{low}}^{E_{upp}}, \quad (7)$$

producing the solutions for electron density N for any given spectral index γ at a given column depth ξ, for pure collisions (Eq. 6), and at a linear column depth s, for pure ohmic losses (Eq. 7).

It can be seen that, similar to Zharkova & Kobylinskij (1992), the total beam abundances integrated over all energies either for pure collisional losses, $N(\xi)$, or for purely ohmic losses, $N(s)$, are linearly proportional to the beam's initial energy flux, which is implictly included into the normalisation coeffciient K(Dobranskis & Zharkova 2015).

In fact, the total densities, $N(\xi)$, of precipitating electron beams loosing their energy in collisions (Eq. 6) decrease proportionally to a column depth as $N(\xi) \approx \xi^{-(\gamma+1)}$ that is similar to the results reported by Zharkova & Kobylinskij (1992) for pure collisional losses. While for the beam electrons loosing their energy in Ohmic losses the total electron abundances, $N(s)$, (Eq. 7) are decreasing with a linear depth s as $N(s) \approx s^{-\gamma}$. Hence, harder electron beams (with smaller γ) will have a smaller density decrease with depth than the softer ones that enforces a further decrease of the abundances, if both the losses are combined.

3 HXR INTENSITY OF ELECTRONS WITH MIXED ENERGY LOSSES (MELS)

As it was shown in section 2 above, by combining iteratively the solutions of the updated CEs for both Coulomb collisions and ohmic losses one can find the semi-analytical solutions for differential densities of precipitating beams with mixed energy losses. This allows us to evaluate the impact of collisional and ohmic losses on the resulting HXR bremsstrahlung emission.

The differential densities, obtained for collisional and ohmic losses cases are converted into the distribution functions f, $f = \frac{N(E,\xi)}{N(E,0)}$ (Dobranskis & Zharkova 2014, 2015). In the calculations we use the fractions of precipitating and returning electrons defined in section 2.4. For comparison, the distribution functions f_N are obtained for the same beam parameters from a numerical Fokker-Planck approach (Siversky & Zharkova 2009).

In order to estimate the HXR intensity, I, for given photon energy ε and viewing angle ψ, the corresponding distribution functions f are integrated by azimuthal angles ϕ (giving the factor 2π before the intergral), pitch angle cosine μ, electron energy η and column depth ξ as follows (Zharkova et al. 2010):

$$I(\varepsilon,\psi) = 2\pi A_x K \times \int_{\xi_{min}}^{\xi_{max}} \int_{\varepsilon}^{\infty} \int_{-1}^{1} f(\xi,\eta,\mu)\, \eta \sigma^H(\eta,\varepsilon,\psi,\mu)\, d\mu d\eta d\xi, \quad (8)$$

where ε is a dimensionless photon energy hv/E_0, σ^H - are the cross-sections for HXR emission with energy ε formed by electrons with given energy and angle parameters and $A_x = \frac{S}{4\pi R}\frac{2E}{m_e}$, where S defines area of a flare and R is a distance to the observer (≈ 1 a.u). In the equation (8) the relativistic cross-sections are used following Bai & Ramaty (1978) with the correction proposed by Zharkova et al. (2010) .

Table 4. Ratios of elecron abundances for mixed energy losses (MEL) obtained for precipitating (MEL-P) and returning (MEL-R) electrons as estimated from numerial simulations with Fokker-Planck approach for different initial energy fluxes (Siversky & Zharkova 2009).

$F_0 = 10^8 erg\, cm^{-2} s^{-1}$	90% MEL-P + 10% MEL-R
$F_0 = 10^{10} erg\, cm^{-2} s^{-1}$	70% MEL-P + 30% MEL-R
$F_0 = 10^{12} erg\, cm^{-2} s^{-1}$	50% MEL-P + 50% MEL-R

3.1 HXR intensities from precipitating and returning electrons

Let us calculate the HXR emission (Eq. 8) produced by electron beams towards an observer by assuming that it is produced a) directly by the returning electrons and b) by the precipitating electrons whose emission is fully reflected from the photosphere (a full albedo effect). In this scenario one can utilize the ratios of the numbers of precipitating-to-returning electrons derived from FPA in the previous section 2.4. For this purpose the differential densities obtained with the updated CE solution for MEL for both precipitating (Coulomb collisions & ohmic losses) (MEL-P) and returning (Coulomb collisions & returning electrons) (MEL-R) beam electrons are combined using the given ratio for their abundances.

The HXR intensities plotted in Fig. 4 and in the supplementary Fig. 4 are obtained for the electron beams with the same parameters as in Fig. 1 (and supplementary Fig. 1, respectively) for the following ratios of precipitating and returning electrons: 100% MEL-P (black line), 90% MEL-P + 10% MEL-R (blue line), 70% MEL-P + 30% MEL-R (green line), 50% MEL-P + 50% MEL-R (magenta line). The intensities calculated from the Fokker-Planck approach are shown by crosses. From Fig. 4 one can see, that the inclusion of returning electrons has a significant effect on the resulting HXR intensity spectra produced jointly by precipitating and returning electrons that is similar to the conclusions derived from the full Fokker-Planck approach (Zharkova & Gordovskyy 2006; Siversky & Zharkova 2009).

It can be observed that for weaker beams the intensity distributions derived by FP solutions are closer to the distributions when a fraction of returning electrons ranges between 10 (supplementary Fig.4a) and 30 percent (supplementary Fig.4b), while for more intense beams the FP curve fits the MEL curve for 50% of returning electrons (supplementary Fig.4c,d). It can be seen that an increase (10%, 30%, 50%) of the returning electron percentage would result in a noticeable decrease by 0.2 of the lower energy spectral index δ_1 (or in steepening of a HXR intensity spectra) for any additional 20% of returning electrons (see Table 4).

For example, a weak hard beam precipitating electrons combined with at least 10% of returning electrons result in a considerable flattening of their HXR intensity spectra at lower and steepening at higher energies (supplementary Fig. 4a). In the case of stronger but still hard electron beams ($\gamma = 3$, supplementary Fig. 4c) the flattening would extend to approximately 40 keV, while for stronger soft electron beams ($\gamma = 7$, supplementary Fig.4d) it would reach approximately 60 keV.

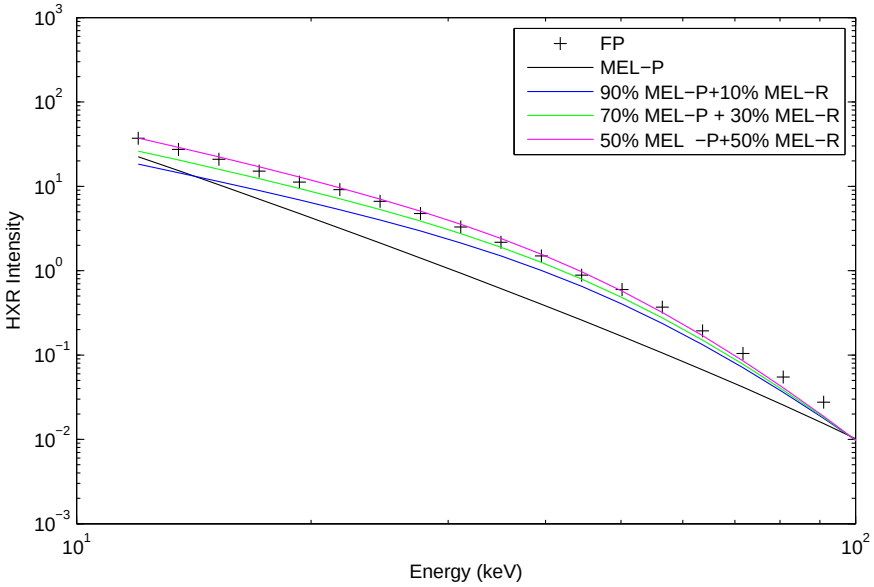

(a) $F_0 = 10^{12} erg\, cm^{-2} s^{-1}, \gamma = 3$

Figure 4. Hard X-ray intensity in relative units, produced by beam electrons loosing their energy in mixed energy losses (MEL) for precipitating (MEL-P) and returning electrons (MEL-R): MEL-P (black line), 90% MEL-P + 10% MEL-R (blue line), 70% MEL-P + 30% MEL-R (green line), 50% MEL-P + 50% MEL-R (magenta line), and from Fokker-Planck approach (crosses). The HXR intensity variations are plotted for low (top row) and high (bottom row) initial energy fluxes of beam electrons and for the beams with hard (left column) and soft (right column) energy spectra.

This explains in very simple analytical terms the similar fundings presented earlier from Fokker-Planck solutions (Zharkova & Gordovskyy 2006; Siversky & Zharkova 2009), describing the HXR intensities, which reflects very non-linear dependence on the parameters of electron beams. In the other words, we demonstrate here that the electron distribution functions formed by the redistribution of precipitating and returning electrons caused by the electric field induced by the precipitating beam itself are accountable for the variations of their resulting HXR intensities. This allows us to derive the beam parameters and the ratio of precipitating to returning electrons from fitting their HXR distributions obtained from observations.

3.2 Fitting to observations the simulated HXR spectra from beams with MELs

3.2.1 Methodology

Using the proposed iterative method for analytical calculation of differential densities for precipitating beam electrons with MEL (section 2.1), one can apply a spectral fitting of the observed HXR emission to those calculated using the MEL distribution functions. This procedure was applied to the main events (emission at the flare footpoints) of nine flares (GOES class C, M and X) summarized in Table 5. The HXR photon energy spectra were obtained for the main HXR bursts in the energy bands from 10 to 100 keV and plotted in Fig.5.

The images are reconstructed using the high-precision PIXON algorithm (Hurford et al. 2002) from the RHESSI branch of SolarSoft (Lin et al. 2002). The integration time was chosen according to a flare class, with 8 *sec* for X-class, 12 *sec* for M-class, and 20 *sec* for C-class flares. Twenty PIXON images were reconstructed for each flare, using the energy bins with logarithmic spacing, ranging from 10 to 100 keV following the methodology described by Hurford et al. (2002). The best image quality, was obtained using the detectors 2 to 7 (front segments only). Then, the thermal component is fitted to the observed photon flux, using fitting routines in the OSPEX application (Hurford et al. 2002; Lin et al. 2002).

Finally, the HXR parts of the photon spectra derived from RHESSI payload are fitted with the HXR emission obtained from CEs for the mixed energy losses (Dobranskis & Zharkova 2015), the original CE for pure collisions and from the numerical Fokker-Planck approach (Siversky & Zharkova 2009).

3.2.2 Fitting the simulated HXR spectra to observations

The results obtained through the spectral fitting using the standard RHESSI methods and the method described in the previous section are presented as a sample in Fig.5 and the supplementary Fig. 5 for 9 flares with the flare parameters summarised in Table 5. The observed HXR intensity is represented by crosses, with the black line defining the thermal component. The same initial energy fluxes are used for electron differential densities derived from the original CE (with pure collisional losses), from the two CEs with MELs using the iterative method decribed in this paper (see section 2.1) and for Fokker-Planck approach using the same MELs.

From Fig.5, one can see a clear increase in the overall HXR intensity with the increasing flare index likely produced by electron beams with a higher initial energy flux.

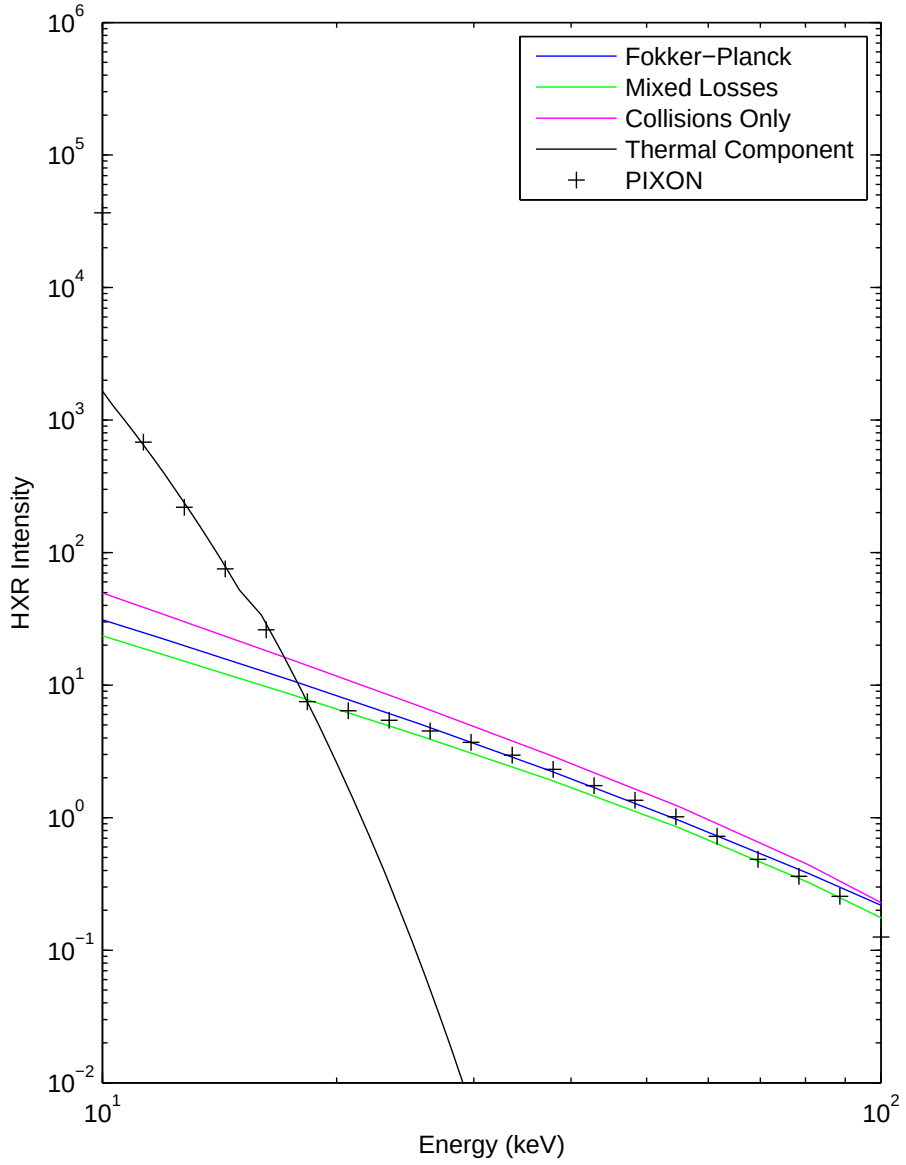

(a) 08 Jan 2014, M3.6 class.

Figure 5. Examples of the HXR photon energy spectra obtained for the main HXR bursts in the energy bands from 10-100 keV for a flare of class M (see for more plots the supplementary Fig. 5) for the flares from the list summarised in Table 5. The fitting is done using a) thermal component (black line); b) the updated CE solutions for Coulomb collisions (magenta); c) the CE solutions for MEL (green) for the relevant ratios of returning and precipitating electron abundances and d) Fokker-Planck solutions for the same beam parameters (blue line). The parameters are compared to the HXR intensity of the flares estimated by PIXON algorithm (crosses) (see the text for details).

For C class flares the HXR emission is observed in the band of 16-18 keV, for M class flares - in the band of 18-20 keV, and for X-class flare - in 27-30 keV. For more powerful flares (or beams) the HXR energy spectra become double power laws. The break in the HXR photon spectra shifts towards higher energies with an increase of the flare class (or an increase of the injected beam initial energy flux).

The investigation of spectral fitting with the different solutions revealed, that the increase of the initial energy flux of beam electrons would increase their resulting HXR intensity. The spectral index used for the mixed energy loss (MEL) model would differ by only 0.1 from the one used with Fokker-Planck approach (FPA). And only in a single case the difference would become 0.2 , for the most powerful flare of 25 October 2013 (GOES class X2.1) (Table 5), which coincides with the conclusions from the previous paper Do-

branskis & Zharkova 2015 (Part 1) (Dobranskis & Zharkova 2015).

The spectral indices of the HXR emission derived from the MEL and Fokker-Planck solutions are presented in the 5th and 6th columns of Table 5 with the ratios of precipitating/returning electrons best fitting the observations shown in the last column. In general, fitting of the observed HXR emission by that simulated for the electrons beams with MELs can be summarised as follows:

(i) For medium (class M) and powerful (class X) flares the proposed joint MEL solutions combining pure collisions and ohmic losses show a closest fit to the observed curves of HXR photon spectra for a particular fraction of returning and precipitating electrons shown in the last column of Table 5.

(ii) For more powerful flares of class X the impact of ohmic losses becomes more pronounced resulting in higher fraction of returning electrons, and thus, in noticeable spectral flattening of HXR intensity at lower energies.

(iii) Spectral indices of the simulated HXR emission derived with the MEL approach are rather close to those derived with FP approach for similar mixed energy losses.

Hence, the MEL approach can explain in very simple terms the spectral flattening towards lower energies by the increased ratio of returning electrons compared to the precipitating ones as pointed by Zharkova & Gordovskyy (2006) and Siversky & Zharkova (2009). In addition, the proposed mixed energy loss approach allows us to derive a preliminary fraction of returning electrons in the whole population in beam electrons, which provides a good starting point for the further Fokker-Planck fitting, if required.

Of course, some discrepancies appearing between MEL and FP approaches can occur due to the fact, that a full pitch angle scattering is not considered in the semi-analytical mixed energy loss approach that can reduce the derived spectral indices compared to those found from FP solutions. Also in the either approach we do not consider magnetic mirroring in converging magnetic field affecting electrons with higher energies that can also slightly reduce the spectral index of resulting HXR emission at higher energies (Zharkova et al. 2011). However, in the four cases out of nine flares considered, the spectral indices derived with the MEL approach are practically identical to FPA, with a difference less than 0.1 (see Table 5).

However, the proposed MEL approach to calculation of electron beam densities and their resulting HXR emission allows any user to reduce by 30-40 times a computation time (a few minutes) required for interpretation of the RHESSI spectra, compared to hours required to calculate distribution functions and HXR emission for a flare using FP approach. This IDL procedure can be easily implemented in the RHESSI software for the benefits of all the RHESSI users.

4 CONCLUSIONS

In this paper we consider the simultaneous analytical solutions of continuity equations for electron beam precipitation a) in collisional losses and b) in Ohmic losses, or mixed energy losses (MELs), by applying the iterative method to calculate the resulting differential densities at given precipitation deph. This approach allows us to provide quick estimations of the contribution of self-induced electric field in the electron beam precipitation and to derive their resulting HXR emission produced by both precipitating end returning electrons forming the electric circuit in solar flares (Zharkova & Gordovskyy 2006; Siversky & Zharkova 2009).

Table 5. Variations of spectral Indices γ of the HXR emission produced by beam electrons with the initial energy fluxes F_0 and ratios of precipitating/returning electrons with the best fit to the RHESSI observations.

Flare Date	Peak	Class	Flux F_0,	MEL γ	FP γ	p/r ratio
	time UT		$erg/cm^2/s$			%
01 Oct 2012	05:03:26	C1.8	$5.2{\cdot}10^8$	3.2	3.2	95/05
17 Jan 2014	08:29:30	C2.2	$6.1{\cdot}10^8$	3.4	3.4	95/05
17 Jan 2014	19:20:22	C7.1	$10.1{\cdot}10^8$	3.6	3.7	90/10
13 Jan 2014	21:51:02	M1.3	$9.7{\cdot}10^{10}$	4.1	4.1	75/25
19 Dec 2013	23:18:26	M3.5	$12.8{\cdot}10^{10}$	4.2	4.3	70/30
08 Jan 2014	03:46:10	M3.6	$13.0{\cdot}10^{10}$	4.3	4.4	70/30
25 Oct 2013	07:59:34	X1.7	$11.6{\cdot}10^{11}$	5.3	5.3	55/45
23 Oct 2012	03:17:22	X1.8	$12.0{\cdot}10^{11}$	5.1	5.2	53/47
25 Oct 2013	15:01:14	X2.1	$12.3{\cdot}10^{11}$	5.2	5.4	50/50

The HXR intensities are compared for the following solutions: the updated CE for Coulomb collisions (Dobranskis & Zharkova 2015), the updated CE for mixed Coulomb collisions & ohmic energy losses (presented here) and the numerical FP solution for Coulomb collisions, ohmic losses and pitch angle scattering (Siversky & Zharkova 2009). In general, HXR bremsstrahlung emission produced by precipitating beam electrons is directed mostly towards the photosphere. Thus, it is considered here to be fully reflected back to the corona (a full albedo effect) (Massone et al. 2004), while the emission of returning electrons is produced directly towards the observer in the top of the atmosphere.

In general, the MEL solutions for differential densities and HXR emission produced by both precipitating and returning electrons can be summarised in the items as follows.

(i) Differential densities (DDs) of precipitating electrons derived from the MEL semi-analytical solutions become much more flattened at lower energies below 10-30 keV compared to the purely collisional case. This flattening becomes stronger with an increasing precipitation depth turning into a positive slope at greater precipitation depths in the chromosphere, producing, thus, a DD distribution with maximum, which shifts towards higher energies with the increase of a column depth.

(ii) From the other hand, the resulting differential densities of combined precipitating and returning electrons are higher at every precipitation depth than those for a pure collisional case. This increases the resulting differential density of beam electrons at a given precipitation depth, which contributes to the HXR bremsstrahlung emission produced towards the top of a flaring atmosphere.

(iii) An overall increase of the differential density of precipitating plus returning electrons is more significant for powerful electron beams, as they induce a stronger electric field, and a larger number of returning beam electrons. Hence, the inclusion of mixed energy losses into the semi-analytical approach proposed here allows us to estimate the

effects of self-induced electric field on electron beam precipitation into flaring atmosphere without running computer-expensive numerical Fokker-Planck simulations.

(iv) A fraction of precipitating and returning electrons is shown to be strongly dependent on the initial energy flux, spectral indices and pitch angle dispersion of electron beam at injection. Weak electron beams are found to have the highest fraction of precipitating electrons being slightly lower for softer electron beams and higher for harder ones. While electron beams with moderate and strong initial energy fluxes there are more electrons accelerated backwards the corona, resulting in a lower fraction of precipitating electrons.

(v) Moreover, the fraction of returning electrons is found to be dependent on a pitch angle dispersion of the beam at its injection on the top boundary. For mildly directed beams (with a pitch angle dispersion of 0.2) an increased number of returning electrons (43-57%) is found at the very top precipitation depths, compared to a much smaller number (¡20%) derived for the narrower beams with a smaller pitch angle dispersion of 0.02.

(vi) Simultaneous consideration of both collisional and ohmic energy losses combining the HXR emission produced by precipitating and returning electrons, reveals a noticeable flattening of their HXR intensity spectra at lower energies (<80 keV). This flattenning is stronger for beams with higher initial energy fluxes, or for more powerful flares.

(vii) Spectral fitting of the HXR emission observed by RHESSI for 9 flares providing the closest fit of the simulated curves to the observed HXR photon spectra helps one to evaluate a fraction of returning electrons versus precipitating ones in these flares shown in Table 5.

(viii) In addition, spectral fitting of the HXR emission found from the MEL approach is very close to the observed HXR photon spectra and with those derived from FP approach within 0.1-0.2.

(ix) As discussed in Introduction, the number of returning electrons can be even further enhanced by a magnetic mirroring, not considered in the current model, while dominating at lower atmospheric depths where the magnetic convergence and magnitude are the highest. This enhancement can noticeably modify the resulting HXR and MW emission for flares with visibly converging magnetic loops that needs to be considered in the future interpretation.

Therefore, the proposed MEL approach can be utilized at the initial investigation stage of spectral fitting providing an opportunity to account simultaneously for both collisional and ohmic losses without lengthy numerical Fokker-Planck simulations. The IDL code implementing the proposed MEL approach can be incorporated into the RHESSI Solar Software for a quicker fit at the initial data processing stage.

ACKNOWLEDGEMENTS

The authors wish to acknowledge that this research is funded by the Science Technology and Facility Council (STFC) project ST/J5000938/1. The authors would like to express their gratitude to the anonymous referee for the constructive and helpful comments, from which the paper strongly benefited. Also RD would like to thank Dr. Eduard Kontar and the Glasgow Astronomy team for their valuable help during his visit to Glasgow, which helped RD to learn working with the RHESSI data and building the HXR spectra for flares of different classes.

REFERENCES

Bai T., Ramaty R., 1978, ApJ, 219, 705
Brown J.C., 1971, Sol. Phys., 18, 489
Brown J.C., 1972, Sol. Phys., 26, 441
Brown J.C., Emslie A.G., Holman G.D., et al., 2006, ApJ, 643, 523
Conway A.J., Brown J.C., Eves B.A.C., Kontar E., 2003, A&A, 407, 725
Courant, R., Hilbert D., 1962, Methods of Mathematical Physics, Methods of Mathematical Physics No. v. 2 (Interscience Publishers)
Diakonov S.V., Somov B.V. 1988, Sol. Phys., 116, 119
Dobranskis R.R., Zharkova V.V., 2014, ApJ, 788, 42
Dobranskis R.R., Zharkova V.V., 2015, MNRAS, 453, 229
Emslie A.G., 1980, ApJ, 235, 1055
Emslie A.G., Holman G.D., Litvinenko Y.E., 2014, ApJ, 792, 5
Haydock E.L., Brown J.C., Conway A.J., Emslie A.G., 2001, Sol. Phys., 203, 355
Holman G.D., Sui L., Schwartz R.A., Emslie A.G., 2003, ApJ, 595, L97
Holman G.D., Aschwanden M.J., Aurass H., et al., 2010, Space Sci. Rev., subm.
Hurford, G. J.; Schmahl, E. J.; Schwartz, R. A.; Conway, A. J.; Aschwanden, M. J.; Csillaghy, A.; Dennis, B. R.; Johns-Krull, C.; Krucker, S.; Lin, R. P.; and 4 coauthors, 2002, Sol.Phys., 210, 61
Knight J.W., Sturrock P.A., 1977, ApJ, 218, 306
Kontar E.P., Brown J.C., McArthur G.K., 2002, Sol. Phys., 210, 419
Kontar E.P., Brown J.C., 2006, ApJ, 653, L149
Kontar E.P., MacKinnon A.L., Schwartz R.A., Brown J.C., 2006, A&A, 446, 1157
Kramers H.A., 1923, 46, 836
Krucker S., Battaglia M., Cargill P.J., et al., 2008, A&A Rev., 16, 155
Leach J., Petrosian V., 1981, ApJ, 251, 781
Leach J., Petrosian V., 1983, ApJ, 269, 715
Lin, R. P.; Dennis, B. R.; Hurford, G. J.; Smith, D. M.; Zehnder, A.; Harvey, P. R.; Curtis, D. W. et al. (another 56 authors), 2002, Sol.Phys., 210, 3
Lin R.P., Krucker S., Hurford G.J., et al., 2003, ApJ, 595, L69
Massone A.M., Emslie A.G., Kontar E.P., et al., 2004, ApJ, 613, 1233
McClements K.G., 1992, A&A, 253, 261
Piana M., Massone A.M., Kontar E.P., et al. 2003, ApJ, 595, L127
Siversky T.V., Zharkova V.V., 2009, A&A, 504, 1057
Sui L., Holman G.D., Dennis B.R., 2005, ApJ, 626, 1102
Sui L., Holman G.D., Dennis B.R., 2007, ApJ, 670, 862
Syniavskii D.V., Zharkova V.V., 1994, Apjs, 90, 729-734
Syrovatskii S.I., Shmeleva O.P., 1972, Soviet Ast., 16, 273
Zharkova V.V., Brown J.C., Syniavskii D.V., 1995, A&A, 304, 284

Zharkova V.V., Gordovskyy M., 2005, A&A, 432, 1033
Zharkova V.V., Gordovskyy M., 2006, ApJ, 651, 553
Zharkova V.V., Kobylinskij V.A., 1992, Kinematics and Physics of Celestial Bodies, 8, 34
Zharkova V.V., Kuznetsov A.A., Siversky, T. V. 2010, A&A, 512, A8+
Zharkova V.V., Meshalkina, N. S.; Kashapova, L. K.; Kuznetsov, A. A.; Altyntsev, A. T., 2011, A&A, 532, A17+